

RESEARCH

Open Access



Anti-EGFR conjugated nanoparticles to deliver Alpelisib as targeted therapy for head and neck cancer

Alberto Juan^{1†}, Carmen Segrelles^{2,3,4†}, Almudena del Campo-Balguerías^{1,5}, Iván Bravo^{1,6}, Ignacio Silva^{2,3}, Jorge Peral², Alberto Ocaña⁷, Pilar Clemente-Casares^{8,9}, Carlos Alonso-Moreno^{1,5*} and Corina Lorz^{2,3,4*}

[†]Alberto Juan and Carmen Segrelles contributed equally to this work

*Correspondence: Carlos.amoreno@uclm.es; clorz@ciemat.es

¹Unidad NanoDrug, Centro Regional de Investigaciones Biomédicas, Universidad de Castilla-La Mancha, 02008 Albacete, Spain

²Unidad de Innovación Biomédica, CIEMAT (ed 70A), Ave Complutense 40, 28040 Madrid, Spain

Full list of author information is available at the end of the article

Abstract

Background: Head and neck squamous cell carcinoma (SCC) is one of the most prevalent and deadly cancers worldwide. Even though surgical approaches, radiation therapy, and therapeutic agents are commonly used, the prognosis of this cancer remains poor, with a tendency towards recurrence and metastasis. Current targeted therapeutic options for these patients are limited to monoclonal antibodies against EGFR or PD-1 receptors. Thus, there is an urgent need to introduce new molecularly targeted therapies for treating head and neck SCC. EGFR can be used as a target to improve the ability of nanoparticles to bind to tumor cells and deliver chemotherapeutic agents. In fact, over 90% of head and neck SCCs overexpress EGFR, and other tumor types, such as colorectal and glioblastoma, show EGFR overexpression. The PI3K/mTOR signaling pathway is one of the most commonly altered oncogenic pathways in head and neck SCC. Alpelisib is a specific PI3K α inhibitor indicated for PIK3CA mutant advanced breast cancer that showed promising activity in clinical trials in head and neck SCC. However, its use is associated with dose-limiting toxicities and treatment-related adverse effects.

Results: We generated polylactide (PLA) polymeric nanoparticles conjugated to anti-EGFR antibodies via chemical cross-linking to a polyethyleneimine (PEI) coating. Antibody-conjugated nanoparticles (ACNP) displayed low polydispersity and high stability. In vivo, ACNP showed increased tropism for EGFR-expressing head and neck tumors in a xenograft model compared to non-conjugated nanoparticles (NP). Alpelisib-loaded nanoparticles were homogeneous, stable, and showed a sustained drug release profile. Encapsulated Alpelisib inhibited PI3K pathway activation in the different cell lines tested that included wild type and altered PIK3CA. Alpelisib-NP and Alpelisib-ACNP decreased by 25 times the half-maximal inhibitory concentration compared to the free drug and increased the bioavailability of the drug in the cells. Herein we propose an efficient strategy to treat head and neck SCC based on nanotechnology.

Conclusions: Anti-EGFR-conjugated polymeric nanoparticles are an effective delivery system to increase drug efficiency and bioavailability in head and neck cancer cells. This strategy can help reduce drug exposure in disease-free organs and decrease drug-associated unwanted side effects.



Keywords: Polymeric nanoparticles, PI3K inhibitors, EGFR, Head and neck cancer, Cancer therapy, In vivo imaging

Background

Head and neck cancer arises in the upper aerodigestive tract. It can affect the lips, oral cavity, salivary glands, larynx, nasopharynx, hypopharynx, and oropharynx. Cancers of the head and neck are the fifth most common worldwide, just after lung cancer, and the seventh leading cause of cancer death. Current figures are discouraging: more than 900,000 people are diagnosed with this type of cancer yearly, and only about half of them will survive the first five years (Cancer Today. International agency for research on cancer WHO, <https://gco.iarc.fr/today/home> (last accessed 21 Sept 2022); Ferlay et al. 2015). More than 90% of head and neck cancers are of a particular type named squamous cell carcinoma (SCC). SCCs also appear in other body locations, including the skin, lungs, bladder, esophagus, and cervix. Recurrence is frequent in head and neck SCC and develops in approximately one-third of the patients. Most patients who experience recurrent or metastatic disease die within a year of diagnosis (Ionna et al. 2021).

Over the last decades, significant advances in surgery and radiation procedures have greatly benefited patients. However, chemotherapeutic and molecularly targeted agents available to treat this type of cancer are scarce. The core of the existing chemotherapeutic arsenal to treat head and neck SCC is based on the use of drugs that widely target DNA (Cisplatin, Fluorouracil) or microtubules (Docetaxel, Paclitaxel) (Price and Cohen 2012). The doses used for these drugs have reached the limit of their safety and tolerability. In fact, because of the frequency of dose-limiting side effects, some patients are not fit for this kind of therapy, and approximately one-third of the eligible patients fail to comply with the complete treatment schedule. In 2006, the monoclonal anti-epidermal growth factor receptor (EGFR) antibody Cetuximab was the first molecularly based therapy introduced for head and neck SCC treatment (Rabney et al. 2006). Since then, thousands of patients have been treated with this therapy with fairly good results and few side effects. More than 90% of head and neck SCCs show increased expression of EGFR. Its overexpression is associated with poor prognosis, metastasis, and resistance to radio and chemotherapy (Johnson et al. 2020; Rabinowits and Haddad 2012). Cetuximab is an important therapeutic option for colorectal cancer (Broadbridge et al. 2012), in which 75% of the patients with metastatic disease have EGFR-expressing tumors. Recently, the avidity of Cetuximab for EGFR on the surface of colorectal tumor cells led to the proposition of a non-invasive in vivo method based on EGFR-targeted molecular imaging for tumor detection and evaluation of chemotherapeutic efficacy (Miyamoto et al. 2019). Gene amplification and overexpression are the most frequent alterations in non-small lung SCC (Cancer Genome Atlas Research 2012), and Cetuximab was used in vitro to deliver gemcitabine to a lung cancer cell line (Wang and Zhou 2015).

Other molecularly targeted therapies are under evaluation to improve clinical outcomes in head and neck SCC. The Phosphoinositide 3-kinase (PI3K) pathway is involved in various biological processes, such as cell cycle progression and survival, and is frequently dysregulated in human tumors (Vivanco and Sawyers 2002). PIK3CA gene codes for the catalytic subunit of PI3K, and it is the most frequently altered oncogene in human tumors (Sanchez-Vega et al. 2018). Alpelisib (BYL719) is an α isoform-specific inhibitor

of PI3K (Fritsch et al. 2014) that is already in clinical use for the treatment of advanced breast cancer with mutations in the PIK3CA gene (Markham 2019), and undergoing clinical trials mostly (other than breast) for head and neck SCC. Alterations in this gene leading to increased activity of the PI3K pathway affect more than half of head and neck SCCs (Cancer Genome Atlas 2015; Garcia-Escudero et al. 2018). In these tumors, over-expression of PIK3CA is associated with poor outcomes (Garcia-Escudero et al. 2018), and alterations in PIK3CA are related to increased sensitivity to Alpelisib (Elkabets et al. 2015). Thus, Alpelisib represents an attractive therapeutic strategy for this tumor type.

Although Alpelisib shows limited toxicity compared to pan-class PI3K inhibitors (Fritsch et al. 2014), treatment with this drug is associated with dose-limiting toxicities and frequent all-grade, treatment-related adverse events. These include hyperglycemia, nausea, decreased appetite, diarrhea, or vomiting, which can negatively affect patients' quality of life, thus impairing long-term administration (Juric et al. 2018). In this regard, nanotherapy could provide solutions by encapsulating therapeutic agents in controlled-release systems. Mizrachi et al. (Mizrachi et al. 2017) reported, for the first time, PI3K inhibition using a fucoidan-based nanodelivery system as a novel approach to mitigate Alpelisib toxicity in head and neck SCC patients. This system showed significant tumor inhibition with non-systemic toxicity.

Herein we report for the first time a tumor cell-targeted approach to deliver a PI3K specific inhibitor using antibody-conjugated nanoparticles (ACNP) as a potential strategy to improve drug uptake and distribution and to reduce drug toxicity in healthy tissues. For this purpose, Alpelisib was encapsulated into polymeric nanoparticles using the FDA-approved compound polylactide (PLA) as raw material, and Cetuximab was conjugated via carbodiimide chemistry over their surface to generate the guided nanoparticles. Alpelisib-loaded EGFR-targeted and non-targeted nanoparticles were fully characterized, and their release profiles and stability in storage were studied. The anti-proliferative effect of the nanoparticles and their capability to inhibit the activation of the PI3K pathway were evaluated. We performed microscopy analysis and *ex vivo* imaging of labeled ACNP to support the hypothesis that Alpelisib-loaded ACNP would be a more specific therapeutic option for head and neck SCC treatment. This work sets the bases for further preclinical studies in head and neck SCC and other types of cancer using EGFR-targeted polymeric nanoparticles.

Results

Formulation and characterization of nanoparticles

We optimized the double emulsion method (Niza et al. 2021) to load PLA nanoparticles (NP) with Alpelisib or the near-infrared fluorescent cyanine dye 1,1'-diiodo-3,3',3',3'-tetramethylindotricarbocyanine iodide (DiR) to generate the loaded nanoparticles NP-Alpelisib and NP-DiR, respectively. Conjugation of loaded and non-loaded nanoparticles with Cetuximab was achieved by chemical cross-linking covalent-coupling of the antibody to a PEI coating to generate the antibody conjugated nanoparticles ACNP-Alpelisib and ACNP-DiR (Fig. 1a, overview of the formulation of Alpelisib-loaded nanoparticles) (Cimas et al. 2020). The characterization of NP and ACNP, both non-loaded and loaded, was carried out by dynamic light scattering (DLS), scanning electron microscopy (SEM), and transmission electron microscopy (TEM).

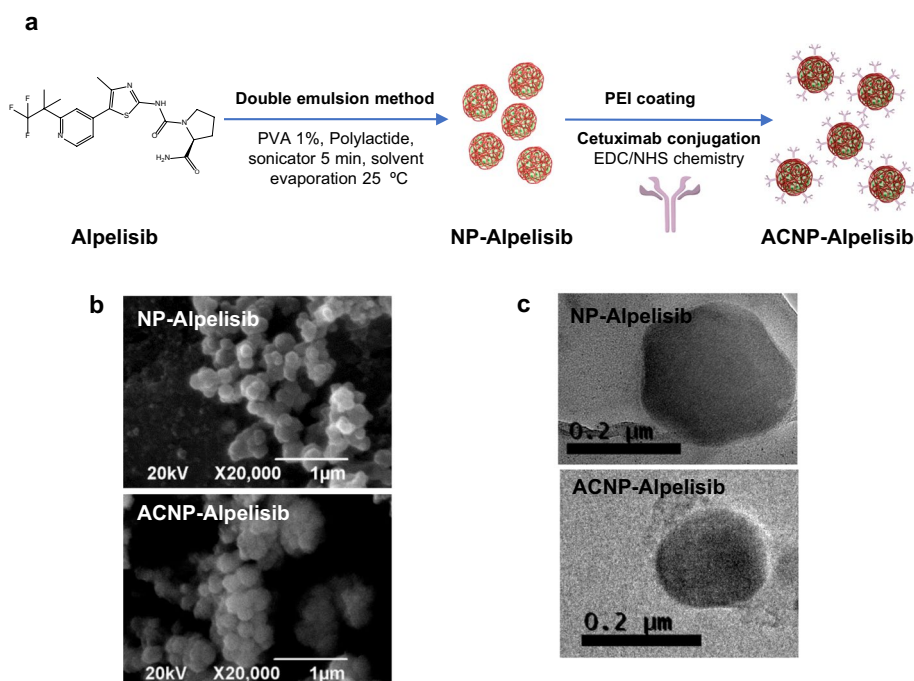


Fig. 1 Formulation and characterization of Alpelisib-loaded nanoparticles. **a** Schematic illustration of the formulation of NP and ACNP loaded with Alpelisib. PVA: polyvinylalcohol; EDC: 1-ethyl-3-(3-dimethylaminopropyl) carbodiimide hydrochloride; NHS: N-Hydroxysuccinimide. **b** SEM and **c** TEM images of NP-Alpelisib and ACNP-Alpelisib. Scale bars: 1 µm **b**, 0.2 µm **c**

Table 1 Characterization of loaded and non-loaded nanodevices

Formulation	R_H (nm)	Pdl	Z-Potential (mV)	EE (%)	LE (%)	Antibody conjugation (%)
NP	113.73±2.40	0.110±0.01	4.05±0.81	–	–	–
NP-Alpelisib	104.60±1.05	0.066±0.02	4.57±0.88	38.34±5.22	4.25±1.20	–
NP-DiR	106.53±1.00	0.112±0.03	3.94±0.95	3.72±0.44	0.41±0.04	–
ACNP	129.70±4.30	0.190±0.08	2.53±0.55	–	–	93±1.80
ACNP-Alpelisib	108.80±0.82	0.126±0.03	9.64±1.18	18.47±1.92	6.84±0.84	85±2.44
ACNP-DiR	131.80±1.31	0.162±0.01	1.98±0.30	2.47±0.22	0.39±0.04	89±2.30

Hydrodynamic radius (R_H), polydispersity index (Pdl), Z-potential, encapsulation efficiency (EE %), and loading efficiency (LE %) of the formulations. Errors are 2σ

The percentage of encapsulation efficiency (EE%) and loading efficiency (LE%) of Alpelisib was calculated according to established protocols (Cimas et al. 2020). The standard protocol of bicinchoninic acid assay (BCA) was followed to quantify the amount of antibody on the surface of the nanoparticles (Cimas et al. 2020). Table 1 collects the physicochemical characteristics of the nanodevices. Size distribution curves for the optimized formulations obtained by DLS revealed similar average particle size of non-loaded and loaded polymeric-based nanoparticles (Additional file 1: Fig. S1). Alpelisib or DiR loading into the nanodevices did not significantly alter the physical parameters of the formulations. Similarly, after optimization of the formulations, ACNP-Alpelisib showed similar LE% compared to its non-conjugated counterparts (Table 1). All formulations

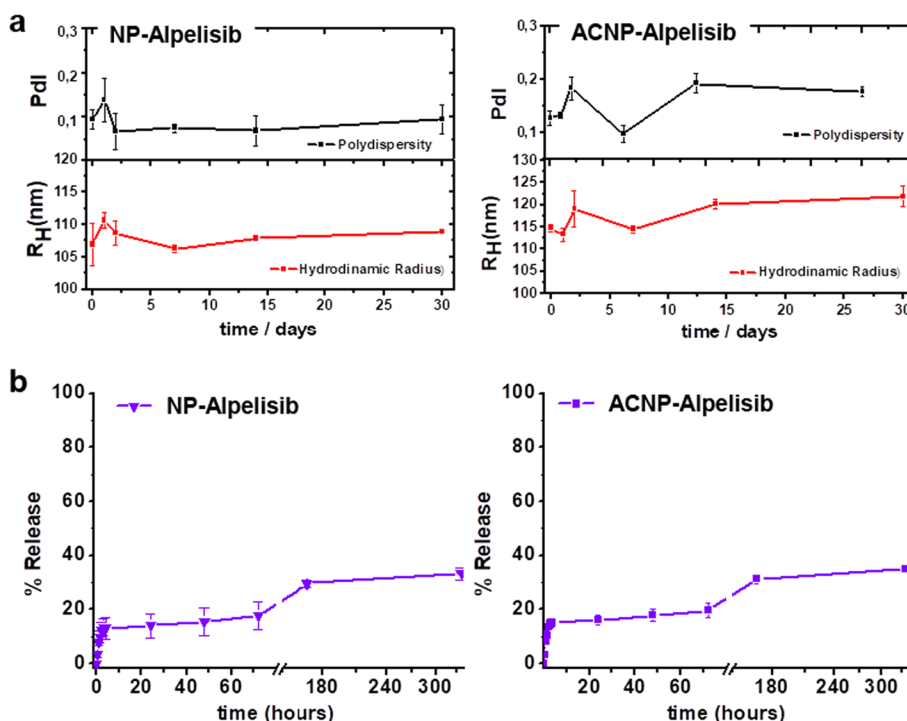


Fig. 2 Storage stability and release profiles for NP-Alpelisib and ACNP-Alpelisib. **a** Storage stability in PBS (pH 7.4) at 4 °C of NP-Alpelisib and ACNP-Alpelisib. **b** In vitro release profiles of NP-Alpelisib and ACNP-Alpelisib in PBS (pH 7.4) at 37 °C. Data are expressed as mean ± SEM from at least three independent experiments

displayed spherical morphology, as shown in representative examples of SEM and TEM images of NP-Alpelisib and ACNP-Alpelisib (Fig. 1b, c). The observed size was similar to that of DLS with uniform size distribution.

Release profiles and storage stability of Alpelisib-loaded nanoparticles

Nanoparticle stability was studied by monitoring the hydrodynamic radius (R_H) and polydispersity index (PdI) values of NP-Alpelisib and ACNP-Alpelisib in PBS over time (Fig. 2a). The increase in either particle size or PdI during a month-long follow-up period was negligible, demonstrating the high stability of both formulations during storage at 4 °C. Next, we studied the release profiles of NP-Alpelisib and ACNP-Alpelisib using the dialysis method at pH 7.4 and 37 °C to mimic physiological conditions. None of these nanoparticles showed a significant burst release. On the contrary, both formulations showed sustained Alpelisib release, with the expected triphasic profile for polymeric nanoparticles (Niza et al. 2021) (Fig. 2b).

Interaction of fluorescent-labeled nanoparticles with tumor cells

To assess the ability of both NP and ACNP to target human cancer cells, we studied the interaction of both nanodevices with the EGFR-expressing human tongue SCC-derived cell line Cal33 (Segrelles et al. 2018). After exposure to different amounts of the fluorescent-labeled nanoparticles, NP-DiR and ACNP-DiR, cells were marked with antibodies against the epithelial cell membrane protein E-cadherin and stained with the nuclear marker 4',6-diamidino-2-phenylindole (DAPI) (Fig. 3a). In both cases, DiR

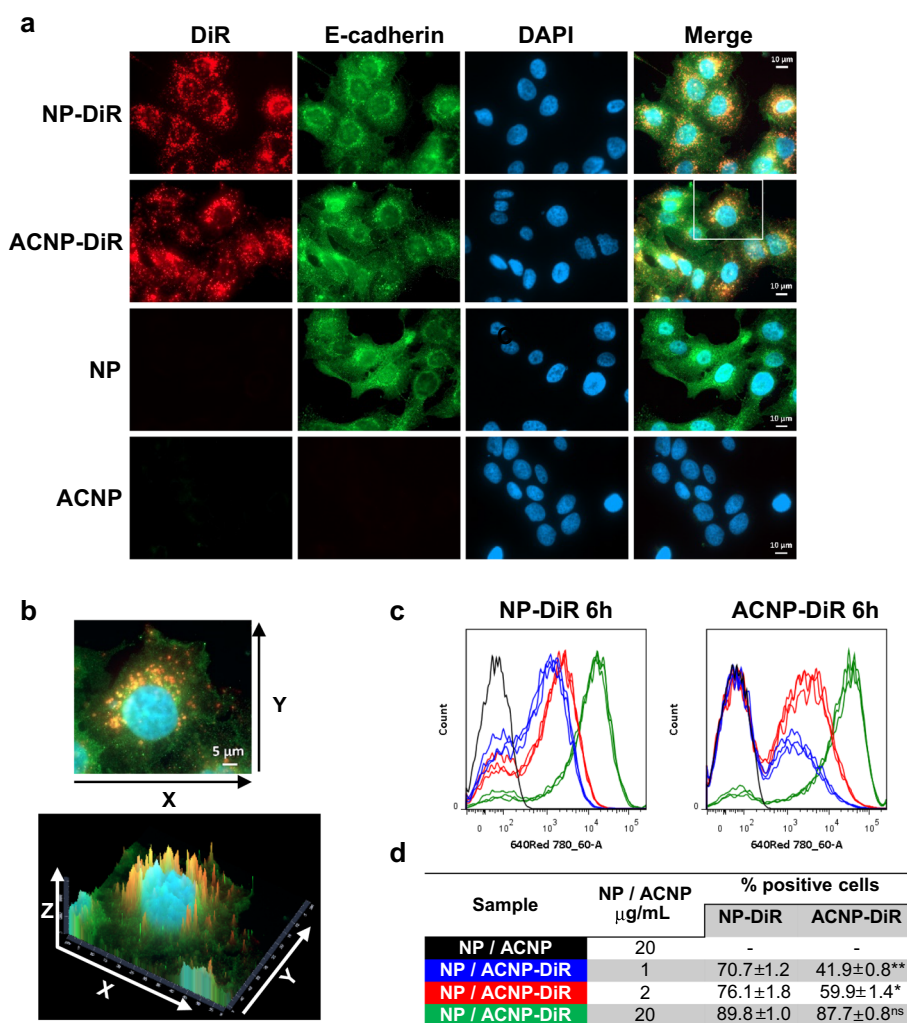


Fig. 3 **a** and **b** Microscopy analysis of the interaction of NP and ACNP (20 $\mu\text{g/mL}$) with Cal33 cells. **a** Nuclei were stained with DAPI and pseudocolored in blue; cell membranes were stained with E-cadherin and pseudocolored in green; and DiR fluorescence signal was pseudocolored in red. Scale bar 10 μm . The images in the lower panel correspond to a sample not incubated with the primary anti-E-cadherin antibody. **b** The upper picture shows a magnification of the square outlined in white in **a**. The lower picture shows its corresponding 2.5D image. X and Y-axis indicate the position and Z-axis shows the fluorescence intensity value of each channel. **c** Flow cytometry histogram overlay plots showing the fluorescence of Cal33 cells treated with 1 (blue), 2 (red), and 20 (green) $\mu\text{g/mL}$ NP or ACNP labeled with DiR for 6 h. The black line denotes unlabeled-cell background fluorescence. A representative experiment of three (with each condition in triplicate). **d** Number of positive cells in each condition. Mean \pm SEM. *pVal* versus NP-DiR at similar concentration: ***pVal* < 0.001; **pVal* < 0.05; ns, not significant

signal associated with membrane and intracellular presence within the cells. Volumetric 2.5D (Ren and Han 2021) surface plots showed that DiR signal formed cytosolic aggregates in the cytoplasm of the cells, particularly in the perinuclear region (Fig. 3b). This is consistent with current evidence that mammalian cells can efficiently take up polymeric nanoparticles (Mazumdar et al. 2021; Niza et al. 2021).

The process of nanoparticle internalization was quantitatively analyzed using flow cytometry (Fig. 3c and Additional file 1: Fig. S2). Cal33 cells were incubated at different time points with several concentrations of DiR-labeled nanoparticles. At short time

points (6 h) and low concentrations of nanoparticles (1 and 2 $\mu\text{g}/\text{mL}$), the number of positively labeled cells was higher in the cultures incubated with NP-DiR compared to ACNP-DiR. However, the percentage of labeled cells was similar at longer incubation times and higher concentrations. These results suggest that, at least in vitro, uptake is similarly efficient for non-functionalized nanoparticles and nanoparticles with Cetuximab, but it might be slightly slower for the latter.

In vivo tumor targeting of fluorescent-labeled nanoparticles in an EGFR-positive SCC xenograft model

The receptor for epidermal growth factor is overexpressed in many cancer types. The Cancer Genome Atlas (TCGA) encompasses molecular (genomic, epigenomic, transcriptomic, proteomic) and clinical data of over 20,000 primary cancer and matched normal (non-tumor adjacent tissue) samples spanning 33 cancer types that are available to the research community. EGFR gene expression data analysis across the TCGA samples using the UALCAN (The University of ALabama at Birmingham CANcer) data analysis portal (Chandrashekar et al. 2017; Chandrashekar et al. 2022) showed that SCCs, including bladder, cervical, esophageal, lung and head and neck, express high levels of the gene. In squamous tumors of the upper aerodigestive tract (esophageal and head and neck), the expression of EGFR is higher than in the corresponding normal tissue and most of the normal tissues analyzed (Additional file 1: Fig. S3A). Protein data from The Cancer Proteome Atlas (TCPA) were consistent with gene expression data and showed that SCCs are among the tumors with the highest EGFR protein abundance (Additional file 1: Fig. S3B). Head and neck SCC tumors express significantly more EGFR than normal tissue at all stages of the disease (Additional file 1: Fig. S4A). These include grade 1 (well-differentiated tumors) (Additional file 1: Fig. S4B) and stage 1 tumors (small tumors, usually <2 cm across, that have not spread to nearby lymph nodes or organs in other parts of the body) (Additional file 1: Fig. S4C).

We used a previously established xenograft model that recapitulates well-differentiated head and neck SCC (Segrelles et al. 2018) to study in vivo tumor targeting of NP and EGFR-targeted ACNP. In this model, the human SCC-derived cell line Cal33 was used to generate subcutaneous tumors in the right flank of immunodeficient mice (Fig. 4a, overview of the xenograft experiment). It has been shown that Cal33-derived xenografts express EGFR, and the anti-EGFR monoclonal antibody Cetuximab efficiently targets this receptor (Elkabets et al. 2015). Tumors of mice injected with ACNP-DiR displayed a higher signal than those injected with NP-DiR (Fig. 4b, c). Therefore, in vivo data indicate that, although ACNP did not show increased uptake by Cal33 cells in vitro, the presence of an EGFR-aiming antibody improves nanoparticle tumor targeting in vivo.

Antiproliferative effect of free Alpelisib and Alpelisib-loaded nanoparticles

In vivo and in vitro data using fluorescent-labeled nanoparticles showed that NP and ACNP are readily taken up by tumor cells and that their functionalization with the anti-EGFR antibody Cetuximab increases in vivo tumor targeting. Next, we tested the ability of these nanocarriers to deliver the specific PI3K α inhibitor Alpelisib into cancer cells.

First, we evaluated the in vitro toxicity of free Alpelisib in three different head and neck SCC-derived cell lines. Then, we compared it to the toxicity induced by the

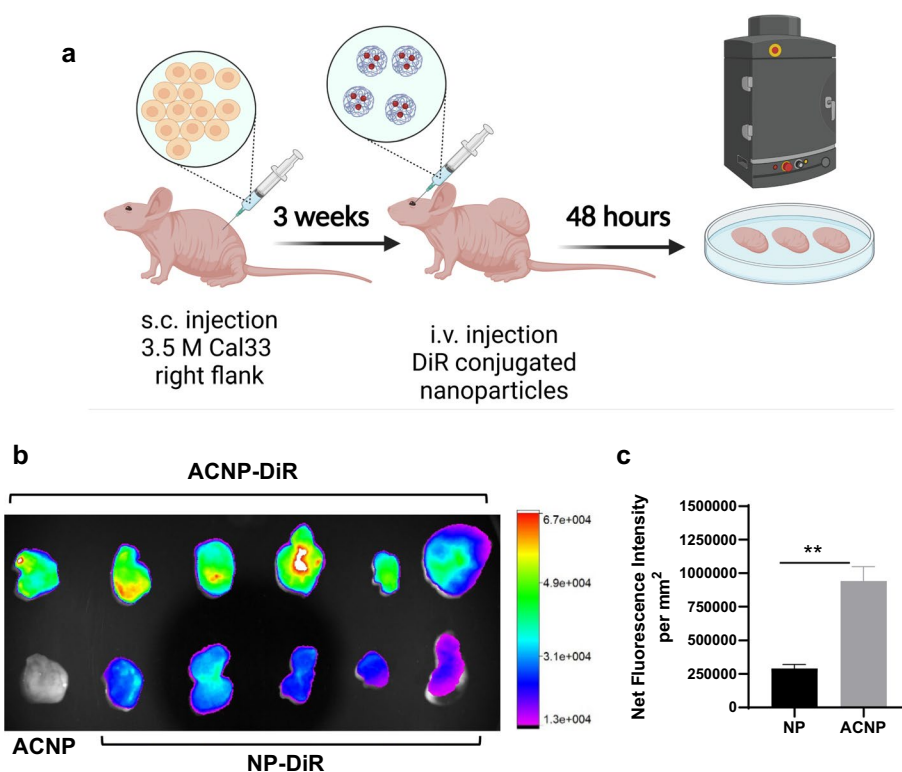


Fig. 4 Tumor targeting of DiR-labeled NP and ACNP in Cal33 xenografts. **a** Mouse xenograft model schematics. The indicated number of Cal33 cells was subcutaneously (s.c.) injected into the right flank of immunocompromised nude mice. After 3 weeks, mice were injected intravenously (i.v.) with 100 μ l of DiR-labeled nanoparticles (NP-DiR and ACNP-DiR) or with non-labeled nanoparticles (ACNP) and ex vivo fluorescence was analyzed 48 h later. **b** Overlay of photographic and fluorescence images of Cal33 tumors from mice injected with the indicated nanoparticles (NP-DiR, ACNP-DiR, and non-labeled ACNP) and analyzed 48 h later. The color scale shows Fluorescence Intensity per mm². Xtreme imaging system. **c** Net Fluorescence Intensity (sum of the background-subtracted pixel values within the region of interest -tumor- divided by its area). The signal from the tumor injected with non-labeled ACNP was subtracted from all sample (NP-DiR and ACNP-DiR) values. Mean \pm SEM. *******pVal* < 0.001

corresponding amount of drug loaded in nanoparticles (Fig. 5). It has been reported that PIK3CA gene alterations (mutation/amplification) predict sensitivity to Alpelisib in head and neck and esophagus SCC cell lines (Elkabets et al. 2015). In this regard, Alpelisib is indicated for the treatment of advanced breast cancer with mutations in the PIK3CA gene. Therefore, we chose three head and neck SCC cell lines with different PIK3CA statuses: Cal33 harbors an activating mutation in the PIK3CA gene, FaDu has an amplification of the PIK3CA gene, and Cal27 is PIK3CA wild type. We determined the inhibitory concentration (IC) 50 of Alpelisib in these cells at 72-h incubation time (Fig. 5a). Cal33 was the most sensitive to the free drug, followed by Cal27 and FaDu. Treatment with Alpelisib encapsulated in NP and ACNP increased the sensitivity of the different cell lines approximately 25 times compared to the free drug (Fig. 5b–d). Empty nanoparticles did not cause cell death at the IC₅₀ concentration range of the encapsulated drug (Additional file 1: Fig. S5A, B). Cetuximab was not toxic to head and neck SCC cells (Additional file 1: Fig. S5C); this has been reported for other cell types (Roncato et al. 2018).

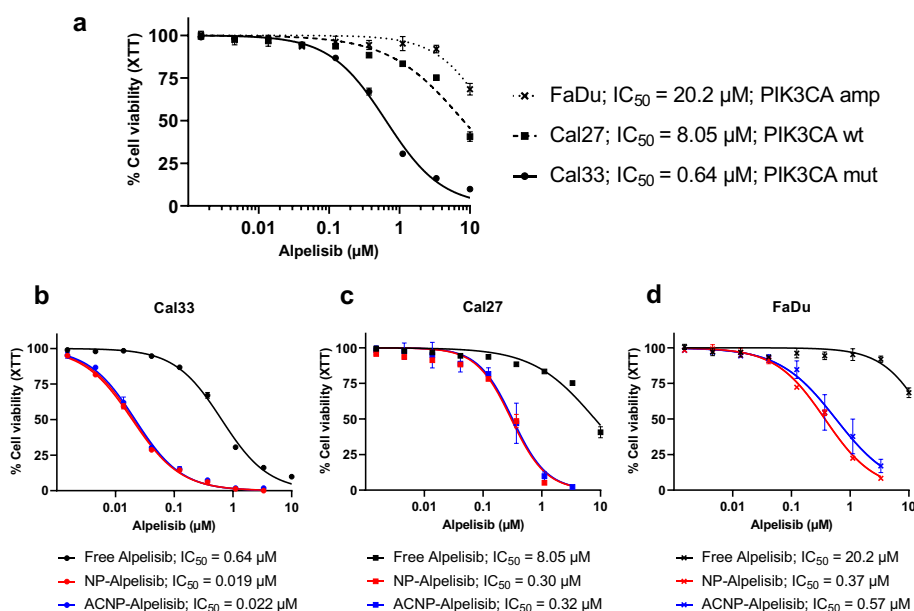


Fig. 5 Antiproliferative effect induced by free Alpelisib and Alpelisib conjugated into nanoparticles in the indicated cell lines at 72 h. **a** Sensitivity of the different cell lines (measured by XTT assay) to free Alpelisib. The inhibitory concentration 50 (IC_{50}) for each cell line is shown. Calculation of the concentrations IC_{50} based on a nonlinear regression curve fit (log(inhibitor) vs. normalized response, variable slope). Cell viability of **b** Cal33, **c** Cal 27, and **d** FaDu cells incubated for 72 h with different concentrations of free Alpelisib (as in **a**) or with equivalent amounts of the drug loaded into NP or ACNP. IC_{50} for each condition is shown. Mean \pm SEM. Curve fit for: NP-Alpelisib or ACNP-Alpelisib versus free drug, $pVal < 0.0001$; NP-Alpelisib versus ACNP-Alpelisib, $pVal > 0.5$ (not significant). Extra-sum-of-squares F test

Our data show that the delivery of Alpelisib in nanoparticles increased the sensitivity to the drug even in the Alpelisib-resistant FaDu cell line. Cell survival inhibition for NP-Alpelisib compared to ACNP-Alpelisib was similar in the three cell lines tested. This observation is consistent with the in vitro uptake kinetics results in Cal33 that showed a comparable capacity to internalize NP and ACNP.

Vehiculation of Alpelisib into NP and ACNP improves its cell bioavailability

A common hindrance of drugs is their bioavailability. The duration of action of a drug entails that the concentration range with therapeutic effect needs to be maintained over time. Plasma-concentration time-profile studies in 5000 patients showed that a total 24-h dose of 400 mg Alpelisib could maintain the IC_{80} on tumor growth in 90% of patients if administered twice daily, but not once daily (De Buck et al. 2014). We showed that Alpelisib vehiculation into polymeric nanoparticles decreased approximately 25-fold the concentration needed to reach an IC_{50} antiproliferative effect compared to the free drug. Since nanoparticles readily enter and accumulate in the cell, we wanted to know whether vehiculation could increase intracellular drug bioavailability. With this purpose in mind, we carried out two parallel analyses (Fig. 6a, overview of the experiment). In one, cells were treated with a low drug concentration (IC_{25} at 24 h, Fig. 6b) or drug-loaded nanoparticles for 24 h. In the other, drug or drug-loaded nanoparticles were removed after a 6-h incubation time, and cells were incubated with drug-free media for another 18 h. Cultures were assayed for cell survival

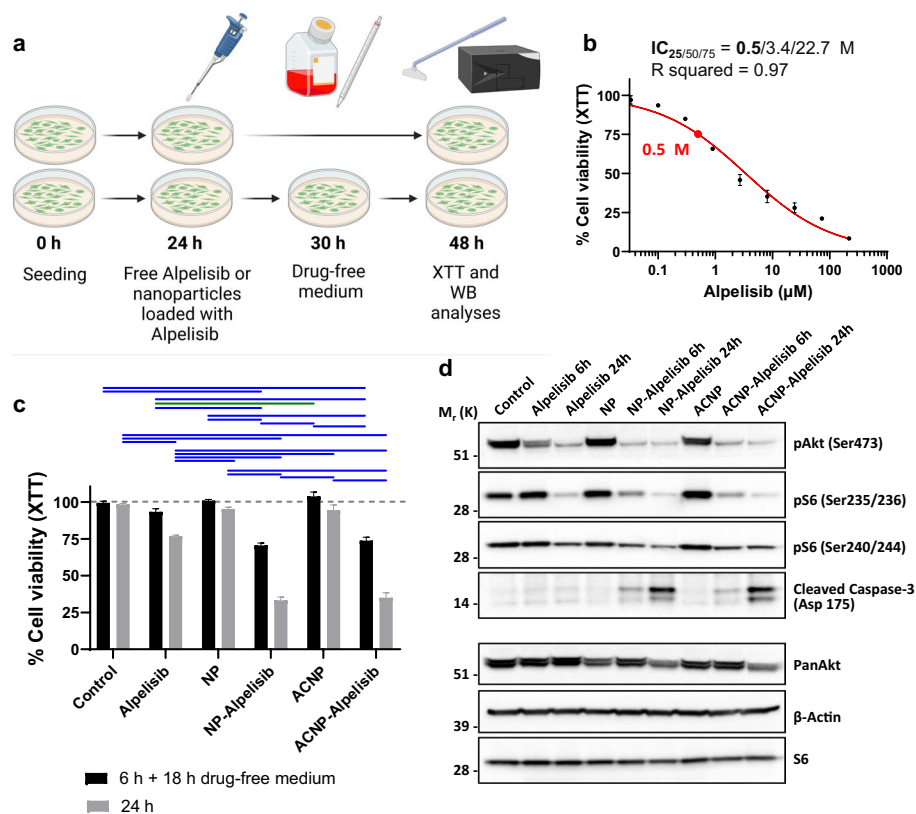


Fig. 6 **a** Schematic illustration of the experiments in **c** and **d**: 24 h after seeding, cells were treated with 0.5 μM free Alpelisib or with the same amount of drug loaded in nanoparticles. The drug was left for 24 h, and cell viability (XTT assay) and proteins (Western blot) were analyzed. In some plates, culture medium was replaced by drug-free medium after 6 h of incubation with the different compounds, and cell viability and proteins were analyzed 18 h later. **b** Cell viability was measured after treatment of Cal33 cells with increasing concentrations of free Alpelisib for 24 h to determine inhibitory concentrations (IC) 25, 50 and 75. R squared: goodness of fit to a Log(inhibitor) vs. normalized response variable slope regression curve. Mean ± SEM. The red dot indicates the concentration used for experiments in **c** and **d** ($IC_{25} = 0.5$ μM). **c** Cell viability analysis of Cal33 cells treated with 0.5 μM free Alpelisib or in nanoparticles for 24 h or for 6 h followed by 18 h incubation with drug-free media. The dotted line indicates 100% cell survival of untreated cells. Control cells were treated with the vehicle of Alpelisib (DMSO). Equivalent concentrations of empty NP or ACNP to nanoparticles loaded with Alpelisib were used. Mean ± SEM. Ordinary one-way ANOVA, Tukey's multiple comparisons test, In blue $pVal < 0.0001$, in green $pVal < 0.05$. **d** Western blot (WB) analysis of the indicated proteins/phosphoproteins

and collected for protein studies at the end of both experiments. Cells treated for 24 h with free Alpelisib (IC_{25}) showed the expected decrease in cell survival ($76.9\% \pm 1.5$). However, 6-h incubation with the free drug did not induce a significant decrease in cell viability (Fig. 6c). In contrast, the delivery of Alpelisib in nanoparticles significantly reduced cell survival already at 6-h incubation time (cell survival: $70.6\% \pm 3.8$ NP-Alpelisib and $73.8\% \pm 5.7$ ACNP-Alpelisib), which further decreased at 24-h incubation time (cell survival: $33.2\% \pm 5.7$ NP-Alpelisib and $35.1\% \pm 8.1$ ACNP-Alpelisib). Importantly, non-loaded nanoparticles did not impair cell growth (Fig. 6c). To ensure the reproducibility of the data, we performed the experiment using different batches of nanoparticles and tested other concentrations of Alpelisib, with similar results (Additional file 1: Fig. S6A, B).

Once inside the cell, Alpelisib must be released from the nanoparticle and retain its activity to exert its function. We showed that Alpelisib-loaded nanoparticles reduced cell survival at lower concentrations and shorter incubation times compared to the free drug. To test the activity of Alpelisib, we examined the activation status (phosphorylation at specific sites) of PI3K-pathway downstream targets Akt kinase and ribosomal protein S6. We also studied the induction of apoptosis (cleaved caspase-3) (Fig. 6d). Treatment with free Alpelisib decreased phosphorylation of the canonical PI3K target Akt at Ser473. This decrease was detected at 6-h and was evident at 24-h incubation with the drug. Treatment with NP-Alpelisib or ACNP-Alpelisib robustly inhibited Akt phosphorylation at short incubation times (6 h). Similarly, the phosphorylation at specific sites (Ser235/236 and 240/244) of the Akt/mTOR downstream target ribosomal protein S6 decreased at short (6-h) incubation times only when the cells were treated with the nanoparticle-loaded drug. Proapoptotic caspase-3 cleavage into an active fragment (cleaved caspase-3 Asp175) was detected only in the cells treated with NP-Alpelisib or ACNP-Alpelisib. Other batches of the nanoparticles were tested for inhibition of PI3K activity and caspase-3 cleavage to exclude batch effects, with similar results (Additional file 1: Fig. S6C). The protein levels of EGFR and its activation status (phosphorylation at Tyr1068) did not change with the different treatments (Additional file 1: Fig. S7).

Discussion

Head and neck SCC is a high-incidence, poor-prognosis cancer for which limited chemotherapeutic options are available (Price and Cohen 2012). Therefore, different molecularly targeted therapies are in evaluation (Johnson et al. 2020). These tumors frequently display aberrant activation of the PI3K/mTOR pathway (Cancer Genome Atlas 2015; Wang et al. 2017), and PI3K inhibitors have shown preclinical activity in head and neck SCC (Massacesi et al. 2016). One of these is the PI3K α -specific inhibitor Alpelisib, which is currently under clinical trials for head and neck SCC (Day et al. 2020; Dunn et al. 2020). Although definitive evidence of clinical activity in this cancer is still pending, data in breast cancer strongly support its use in tumors with PIK3CA alterations. Despite showing less toxicity than other pan-class PI3K inhibitors, dose-limiting side effects and long-term tolerability hamper its clinical use (Juric et al. 2018). Several combination regimens reducing the maximum tolerated dose of Alpelisib are under study to overcome the above limitations (Day et al. 2020; Dunn et al. 2020). To our knowledge, systems aimed to deliver Alpelisib to the tumor cells have not been explored in depth as a therapeutic option in head and neck SCC. Selective targeting of tumor cells can augment the penetration of the nanocarriers within the tumor, decreasing the toxicity and the adverse effects of high doses or prolonged treatment. Only the work of Mizrachi et al. in 2019 reported successful results by encapsulating Alpelisib in polysaccharide-based nanoparticles conjugated with fucoidan. They showed that fucoidan displays an affinity for the cell adhesion molecule P-selectin, expressed in the vasculature of head and neck tumors. However, some tumors need to be irradiated to induce P-selectin expression, so P-selectin might not always be a suitable target.

Targeted therapies, such as Alpelisib, can be encapsulated into nanocarriers that can be guided to the tumor through conjugation with antibodies, the so-called antibody-conjugated nanoparticles (ACNP). The growth receptor EGFR is broadly

overexpressed in head and neck SCC and antibodies against this receptor (Cetuximab) are in clinical use. With this strategy in mind, Alpelisib was encapsulated in polymeric nanoparticles and conjugated to the anti-EGFR monoclonal antibody Cetuximab to generate, for the first time, Alpelisib-loaded ACNP. To facilitate a prompt translation to the clinic, we used FDA-approved PLA as raw material to generate the polymeric nanoparticles formulated following the double emulsion method (Niza et al. 2021). The formulation of Alpelisib-NP and Alpelisib-ACNP was optimized to yield nanoparticles of R_H close to 100 nm with a very narrow polydispersity (Table 1). SEM images correlated with DLS measurements, and the morphology previously observed for polymeric nanoparticles was confirmed by TEM (Fig. 1). The functionalization of nanoparticles with Cetuximab was carried out via covalent-nature binding. The chemistry of carbodiimide is the most commonly used covalent conjugation due to its low cost and high efficiency, which could help manufacturing control procedures (Juan et al. 2020). The carboxyl groups of Cetuximab were activated by the addition of the cross-linking agents EDC and NHS to improve coupling through the primary amines of the surface of the nanoparticles provided after PEI-coating. A BCA assay showed that the conjugation procedure was highly efficient. Loading efficiencies were in accordance with the encapsulation of drugs in PLA-core nanoparticles. Notably, Alpelisib loading or conjugation with Cetuximab did not alter nanoparticle properties or their stability over time. All combinations, with and without Cetuximab conjugation, were very stable formulations. Nanoparticles exhibited controlled release of Alpelisib. In the first stage, both formulations (NP and ACNP) showed a short burst release at pH 7.4; in the second stage, a sustained drug release profile was observed. The erosion of the polymer may govern the last and slower delivery stage. These triphasic release profiles are usual for polymeric nanoparticles (Niza et al. 2021).

The near-infrared fluorescent DiR dye was encapsulated in nanoparticles to evaluate their cell-targeting properties. 2D image microscopy of head and neck SCC cells incubated with DiR-loaded nanoparticles and stained with the epithelial marker E-cadherin showed that both NP and ACNP readily enter the cells. Single-cell volumetric 2.5D images (Ren and Han 2021) revealed that the fluorescent-labeled ACNP form cytosolic aggregates in the cytoplasm and the area surrounding the nuclei of the cells. This suggests their localization in the lysosomal compartment, as previously reported for this type of nanoparticles (Mazumdar et al. 2021; Niza et al. 2021). The efficiency of nanoparticle uptake was measured by flow cytometry. Cells treated with empty or DiR-labeled nanoparticles were analyzed and the percentage of fluorescent positive cells (compared to background fluoresce of cells treated with empty nanoparticles) for the different conditions was determined. Even at short incubation times (6 h), more than 85% of the cells incubated with DiR-labeled nanoparticles were positive. The remaining negative cells were possibly undergoing cell division at that moment. At a longer incubation time, more than 95% of the cells were positive. At high concentrations of nanoparticles or long incubation times, *in vitro* uptake of DiR-ACNP was comparable to DiR-NP. However, the uptake of DiR-ACNP at short incubation times or low concentrations of nanoparticles was slightly less efficient than DiR-NP. This was in contrast with the uptake profiles in mice, suggesting that the presence of the antibody over the surface of the nanoparticle improves *in vivo* tumor targeting.

The *in vivo* xenograft animal models clearly showed an enhanced tropism of the ACNP for the tumors compared to the NP. However, Cetuximab does not recognize murine EGFR, so this model does not allow the analysis of the tropism of the ACNP for tissues that express (murine) EGFR in the animal. For this purpose, NP conjugated with an antibody recognizing the murine EGFR should be used.

More than 55% of head and neck SCC display alterations in the PIK3CA gene, including activating mutations, amplification, and overexpression of the gene, which contribute to the activation of the PI3K pathway (Garcia-Escudero et al. 2018). Therefore, head and neck SCC cell lines with different PIK3CA statuses were treated with Alpelisib-loaded nanocarriers. As expected, PIK3CA mutant cells were the most sensitive to free Alpelisib (Elkabets et al. 2015), and encapsulation of Alpelisib in the nanoparticles further enhanced this effect. Moreover, when encapsulated, cells resistant to the dose range used of the free drug presented similar sensitive profiles to mutant cells treated with the free drug. The ability of the encapsulated drug to induce cell death in resistant head and neck SCC is a promising finding that suggests that this could be a valid strategy for tumors initially resistant to Alpelisib.

Strategies aimed at reducing the drug dose and exposure time needed to achieve a relevant clinical effect are of great interest since they are likely to increase the efficacy of the drug while diminishing its unwanted side effects. To test whether delivery of Alpelisib using PLA-polymeric nanoparticles could improve its bioavailability, we exposed the cells to similar concentrations of free or conjugated drug for a short time (6 h) and then withdrew Alpelisib from the culture. Our results showed that, in this condition, encapsulated Alpelisib was able to reduce cell viability significantly, induce apoptotic cell death (cleaved caspase-3), and block the activation of the PI3K downstream targets Akt and ribosomal protein S6. It required 24 h of incubation with the free drug to achieve comparable outcomes. These results show that encapsulation in nanoparticles enhances drug uptake, which concentrates inside the cells, possibly in lysosomes, and is then slowly released causing a long-lasting inhibitory effect on the PI3K pathway. Thus, encapsulation in PLA-polymeric nanoparticles could help to improve the pharmacological properties of Alpelisib, opening the way for the safer use of this drug.

Conclusions

This is the first time that a tumor cell-targeted approach based on ACNP is used to deliver a PI3K-specific inhibitor. Our *in vivo* and *in vitro* results show that encapsulation of Alpelisib in antibody-conjugated (EGFR-targeted) PLA-polymeric nanoparticles could help to improve drug uptake and distribution, opening the way for its safe use in head and neck SCC. Similarly, the Alpelisib-loaded EGFR-targeted nanoparticles described here could be used in the context of other EGFR-expressing tumors with alterations in PI3K, such as colorectal cancer and lung SCC.

Material & methods

Chemicals

Poly-*rac*-lactide (22,000 kDa) (PLA) was synthesized by Ring-Opening Polymerization (ROP) using Schlenk techniques under argon atmosphere (Sanchez-Barba et al. 2009). Zinc catalyst was prepared following literature procedures (Sánchez-Barba et al.

2007). *Rac*-Lactide, 1-ethyl-3-(3-dimethylaminopropyl) carbodiimide hydrochloride (EDC) (HPLC \geq 98% purity), N-Hydroxysuccinimide (NHS) (HPLC \geq 98% purity) and pluronic[®] F-127 were purchased from Sigma-Aldrich (Darmstadt, Germany). DiR (HPLC $>$ 99%) was purchased from Biotium (Freemont, CA, USA). Alpelisib (BYL719) (HPLC \geq 99.9%) was purchased from MedChemexpress (MedCem Express, Monmouth Junction, NJ, USA). Cetuximab was from Merck (Darmstadt, Germany).

Formulation of nanoparticles

Formulation of polymeric nanoparticles and their loading with Alpelisib or DiR. Loaded nanoparticles were formulated by double emulsion method (Niza et al. 2021). Briefly, 1 mg of Alpelisib or DiR and 10 mg of PLA were poured into a falcon tube and dissolved in 4 mL of dichloromethane. MilliQ water 1 mL of was added dropwise to the solution and the mixture was gently stirred and homogenized in a Hielscher UP200S sonicator homogenizer for 1 min. The pre-emulsion was poured into a 10 mL solution of polyvinyl alcohol (PVA) 1% w/v and the organic solvent removed under stirring at room temperature. Finally, the nanoparticles were collected after centrifugation for 20 min at 15,000 rpm (\cong 15,093 RCF) at 4 °C.

Formulation of ACNPs. Briefly, 1 mg of Alpelisib or DiR and 10 mg of PLA were poured into a falcon tube and dissolved in 4 mL of dichloromethane. MilliQ water 1 mL of was added dropwise to the solution and the mixture was gently stirred and homogenized in a sonicator homogenizer for 1 min. The pre-emulsion was poured into a 10 mL solution of PVA 1% w/v and 0.5% w/w of PEI and the mixture was gently stirred and homogenized in a sonicator homogenizer for 5 min. The organic solvent was removed under stirring at room temperature. Finally, the nanoparticles were collected after centrifugation for 20 min at 15,000 rpm at 4 °C. Cetuximab (0.074 mg/mL in 0.1 M PBS, pH 7.4) was activated in 4 mL of PBS (0.1 M, pH 5.8) using 40 mg of EDC and 9.7 mg of NHS. Then, PEI-coated Alpelisib- or DiR-loaded NP suspension in PBS pH 5.8 were added to the activated Cetuximab and left for 3 h at room temperature. Finally, the loaded ACNPs were collected after centrifugation for 20 min at 15,000 rpm and 4 °C.

Physicochemical characterization of nanoparticles

Nuclear magnetic resonance (NMR) spectra of PLA obtained by ROP were recorded on a Varian Inova FT-400 spectrometer. Gel Permeation Chromatography (GPC) spectra were analyzed on a PL-GPC-220 instrument (Additional file 1: Fig. S8). Size, Pdl, and Z-potential of nanoparticles were analyzed by DLS technique on a Zetasizer Nano ZS instrument (Malvern Instruments, Marvern Panalytical, Malvern, UK)). Data were analyzed using the multimodal number distribution software included with the instrument. The morphology of nanoparticles was studied by TEM and SEM. SEM images were recorded on a Jeol 6490LV electron microscope at 20 kV. Before their analyses, NP and ACNP were diluted in distilled water, left to air-dry on SEM stubs and coated with Au-Pt using a SC7620-Quorum Technologies sputter coater. Coating is required to avoid charging-up problems on the specimen surface and to achieve good image resolution. Higher resolution images were acquired with a Jeol JEM 2100 TEM microscope operating at 200 kV and equipped with an Oxford Link EDS detector. Prior to TEM observation, NP and ACNP were diluted in distilled water, deposited on Cu microscope grids

and left to air-dry. To avoid damage to the specimens as a consequence of beam irradiation, low-dose conditions were used for the observation. Images were analyzed using Digital Micrograph™ software from Gatan (Pleasanton, CA, USA).

Stability of nanoparticles

Alpelisib-loaded NP and ACNP were stored over time at 4 °C, and incubated at 37 °C (1 mg/mL) in PBS for DLS measurements (average size (nm) and PDI).

Drug-release studies

Lyophilized Alpelisib-loaded NP and ACNP were sealed in a dialysis membrane (3500 Da) and suspended in 10 mL of PBS (pH 7.4). Release media 3 mL were taken out and replaced by fresh medium at regular intervals to measure drug concentration using a spectrophotometer at 275 nm. The UV-Vis absorption spectra were recorded at room temperature using a Cary 100 spectrophotometer (Agilent, Madrid, Spain) using a slit width of 0.4 nm and a scan rate of 600 nm/min. The experiment was carried out 3 times.

Conjugation quantification

Standard protocol of the Bicinchoninic acid assay (BCA) was employed to quantify the concentration of antibodies (Cimas et al. 2020). ACNP samples were incubated in a 96-well plate with a BCA solution for 30 min in the dark. Then, the supernatant was taken out to measure the concentration of non-conjugated antibodies using a spectrophotometer at 563 nm. Independent experiments were carried out 3 times and standard deviation calculated.

Encapsulation and loading efficiencies

Loading efficiency (LE) and encapsulation efficiency (EE) of nanoparticles were determined using the nanoparticle destruction method (Cimas et al. 2020; Juan et al. 2022) and calculated by means of the following equations:

$$LE \% = (\text{weight of encapsulated Alpelisib or DiR (mg)}) / (\text{weight of total (Alpelisib or DiR encapsulated + scaffold weight) (mg)}) \times 100\%$$
$$EE \% = (\text{weight of encapsulated Alpelisib or DiR (mg)}) / (\text{weight of Alpelisib or DiR feeding (mg)}) \times 100\%$$

Independent experiments were carried out 3 times and standard deviation calculated.

Cell lines

Three human head and neck SCC-derived cell lines were used: Cal33 (tongue SCC), Cal27 (tongue SCC) and FaDu (pharynx SCC). Cal33 and Cal27 were kindly provided by J. Silvio Gutkind (Department of Pharmacology and Moores Cancer Center, University of California, San Diego, La Jolla, CA, USA) and were originally from ATCC (Rockville, MD, USA). Both cell lines were authenticated based on SNP profiling upon arrival to our laboratory. We purchased FaDu directly from ATCC. The molecular characteristics of these cell lines, including PIK3CA gene mutation/amplification are as described in (Martin et al. 2014 and Elkabets et al. 2015). Cells were cultured in Dulbecco's Modified Eagle's Medium (DMEM, Gibco, Thermo Fisher Scientific, Waltham, MA, USA) supplemented with 10% (v/v) fetal bovine serum (FBS, Gibco)

and 1% (v/v) penicillin–streptomycin (Gibco). All cells were maintained at 37 °C in an atmosphere of 5% CO₂ and 95% humidity. Cell cultures were routinely tested for mycoplasma using a PCR-based detection kit (Venor™ GeM, Sigma-Aldrich).

Microscopy

Tongue SCC Cal33 cells were seeded on Nunc-LabTek chamber slides (Thermo Fisher Scientific). When they reached semiconfluency they were treated with 20 µg/mL unlabeled or DiR-labeled NP or ACNP for 24 h. Slides were fixed in 4% buffered formalin, washed with PBS, incubated for 1 h with blocking buffer (4% bovine serum albumin + 5% horse serum in PBS), then overnight at 4 °C with anti-E-Cadherin (dilution 1:50, clone 36, BD Transduction Laboratories, Becton Dickinson, Franklin Lakes, NJ, USA), followed by incubation with a secondary anti-mouse Alexa Fluor-488 antibody (dilution 1:1000, Invitrogen, Thermo Fisher Scientific). Nuclei were stained with DAPI and mounted with Mowiol (Sigma-Aldrich). Pictures were taken using a Zeiss AxioImager (Zeiss, Oberkochen, Germany) microscope analyzed using ZEN lite software (Zeiss) to obtain 2D and 2.5D images. Volumetric 2.5D images are pseudo 3D images obtained by projecting volumetric information onto a 2D image plane in a single shot through engineering the emitted fluorescence light (Ren and Han 2021).

Flow cytometry

To quantify the interaction of the nanoparticles with the cells, 250,000 Cal33 cells per well were seeded in 12-well plates. After 24 h in culture, they were treated with different concentrations of DiR-labeled nanoparticles for 6 and 14 h. Cells were analyzed using the 640Red 780_60-A laser of a BD LSR Fortessa cell analyzer with BD FACS-Diva Software (BD Biosciences, Franklin Lakes, NJ, USA). Further data analysis was performed with FlowJo software (BD Biosciences). Each experiment was done at least twice, with three replicates per experiment. The fluorescent signal of cells incubated with non-labeled nanoparticles was used to set the threshold (0% positive events).

Mouse xenograft model and comparative analysis of nanoparticle tumor homing

UA previously described tumor-derived cell line xenograft mouse model was used (Segrelles et al. 2018; Velazquez-Lam et al. 2022) (Fig. 4). Briefly, Cal33 cells were trypsinized and suspended in a mixture (2:1) of PBS with Matrigel (BD Biosciences). Three and a half million Cal33 cells suspended in a total volume of 150 µl of PBS-Matrigel were subcutaneously injected in the right flank of (n=12) 10 week old immunocompromised nude (nu/nu) female mice (Janvier, Saint-Berthevin, France). After 3 weeks all mice developed tumors. At this point the mice were injected intravenously with 100 µl of DiR-labeled nanoparticles (≈6.4 µg DiR/mouse) and ex vivo fluorescence in the tumors was analyzed 48 h later using Xtreme In Vivo imaging system (Bruker, Ettlingen, Germany). All animal experiments were conducted in compliance with Institutional Animal Care and Use Committee guidelines and approved by the Animal Welfare Department (reference: PROEX 045.8/21).

Cell survival analysis

For cell survival analysis, Alpelisib was suspended in Dimethyl sulfoxide (DMSO) to a stock concentration of 10 mg/mL (22.6 mM). Cells (10,000 per well) were plated in 96-well plates. After 24 h they were treated with escalating concentrations of free Alpelisib or Alpelisib-loaded nanoparticles at the indicated time points. Cell viability was evaluated with the colorimetric assay XTT Cell Proliferation Kit II (Roche, Basel, Switzerland) following the manufacturer's instructions. Background absorbance (culture medium without cells) was subtracted, and the data were normalized as percentage of control. Each experiment was performed at least three times, and each concentration point was replicated three to six times within each experiment. The corresponding Inhibitory Concentration 50 (IC₅₀) was calculated with GraphPad Prism5 (GraphPad Software, San Diego, CA, USA). This value is defined as the concentration of drug causing a decrease of 50% in cell viability as measured by XTT.

Western blotting

Protein extracts were obtained using a lysis buffer (Hepes 40 mM, Triton-100 2%, β -glycerophosphate 80 mM, NaCl 200 mM, MgCl₂ 40 mM, EGTA 20 mM) supplemented with protease and phosphatase inhibitor cocktails (Roche). Proteins were separated in 4–12% NuPAGE polyacrylamide gels (Invitrogen, Carlsbad, CA, USA) and then transferred to nitrocellulose membranes (GE Healthcare, Little Chalfont, UK) under wet conditions. Membranes were blocked in 5% non-fat milk in TBS-Tween (Tris-HCl 20 mM, NaCl 137 mM, 0.5% Tween) and then incubated overnight at 4 °C with the corresponding primary antibodies in 2.5% BSA TBS-Tween. Peroxidase-coupled secondary antibodies were used specific for rabbit IgG (Amersham, Cytiva, Amersham, UK) and mouse IgG (Jackson, West Grove, PA, USA). Protein bands were detected using Super Signal Western Picoluminescence Substrate (Pierce, Thermo Fisher Scientific) according to the manufacturer's instructions. Images were obtained using a Bio-Rad ChemiDoc MP Imaging System (BioRad, Hercules, CA, USA) and analyzed with Image Lab 6.1 software (BioRad). To avoid cross-signal contamination in the analysis of protein phosphorylation, equal amounts of each protein lysate were loaded on two different gels and run in parallel. One of the gels was blotted with antibodies against the phosphorylated residues of the protein and the other with antibodies recognizing the total form of the protein. Primary antibodies against the following proteins of phosphoproteins were used: p-Akt Ser473 (clone D9E), p-S6 Ser235/236, p-S6 Ser240/244 (clone D68F8), S6 (clone 54D2) and Cleaved Caspase-3 (Asp175) from Cell Signaling (Danvers, MA, USA); and panAkt (clone Y89) and β -actin (clone AC-15) from AbCam (Cambridge, UK). Complete (uncropped) blots are shown in Additional file 1: Figs S9 and S10.

Statistical analysis of the data

Data are shown as mean \pm standard error of the mean (SEM). The Kolmogorov–Smirnov test was run to test the normality of the data. Multiple comparisons analysis was performed using the Kruskal–Wallis test versus control sample or Tukey's multiple comparisons test for ordinary one-way ANOVA. Extra-sum-of-squares F test was

used to compare the goodness-of-fit of two alternative non-linear regression models.
 $*0.001 \leq pVal < 0.05$; $**0.0001 \leq pVal < 0.001$; $***pVal < 0.0001$.

Abbreviations

ACNP	Antibody-conjugated nanoparticle
BCA	Bicinchoninic acid assay
BSA	Bovine serum albumin
DLS	Dynamic light scattering
EDC	1-ethyl-3-(3-dimethylaminopropyl) Carbodiimide
EE	Encapsulation efficiency
FBS	Foetal bovine serum
GPC	Gel permeation chromatography
HPLC	High performance liquid chromatography
RH	Hydrodynamic radius
LE	Loading efficiency
mTOR	Mammalian target of rapamycin
NP	Nanoparticle
NHS	N-hydroxysuccinimide
PBS	Phosphate-saline buffer
PLA	Poly lactide
PVA	Polyvinyl alcohol
PdI	Polydispersity index
PEI	Polyethyleneimine
SEM	Scanning electron microscopy
SCC	Squamous cell carcinoma
TEM	Transmission electron microscopy
DAPI	4',6-Diamidino-2-phenylindole
DMSO	Dimethyl sulfoxide

Supplementary Information

The online version contains supplementary material available at <https://doi.org/10.1186/s12645-023-00180-z>.

Additional file 1: Figure S1. DLS size distribution curve for A) NP, B) ACNP, C) NP-DiR, D) ACNP-DiR, E) NP-Alpelisib and F) ACNP-Alpelisib. **Figure S2.** A) Flow cytometry histogram overlay plots showing the fluorescence of Cal33 cells treated with 1 (blue), 2 (red), and 20 (green) $\mu\text{g}/\text{mL}$ NP or ACNP labeled with DiR for 14 hours. The black line denotes unlabeled-cell background fluorescence. B) Table showing the number of positive cells in each condition. Mean \pm SEM. pVal versus NP-DiR at similar concentration: * pVal < 0.05; ns, not significant. **Figure S3.** EGFR gene expression (A) and protein abundance (B) across The Cancer Genome Atlas (TCGA) tumors. Gene expression (RNAseq) data were downloaded from UALCAN (<http://ualcan.path.uab.edu/analysis.html>) and protein (RPPA) data from The Cancer Proteome Atlas (https://tcpportal.org/tcpa/my_protein.html). A Red bars indicate tumor tissue, in blue normal tissue. Adrenocortical carcinoma (ACC); Bladder Urothelial Carcinoma (BLCA); Breast invasive carcinoma (BRCA); Cervical squamous cell carcinoma and endocervical adenocarcinoma (CESC); Cholangiocarcinoma (CHOL); Colon adenocarcinoma (COAD); Lymphoid Neoplasm Diffuse Large B-cell Lymphoma (DLBC); Esophageal carcinoma (ESCA); Glioblastoma multiforme (GBM); Head and Neck squamous cell carcinoma (HNSC); Kidney Chromophobe (KICH); Kidney renal clear cell carcinoma (KIRC); Kidney renal papillary cell carcinoma (KIRP); Acute Myeloid Leukemia (LAML); Brain Lower Grade Glioma (LGG); Liver hepatocellular carcinoma (LIHC); Lung squamous cell carcinoma (LUSC); Lung adenocarcinoma (LUAD); Mesothelioma (MESO); Ovarian serous cystadenocarcinoma (OV); Pancreatic adenocarcinoma (PAAD); Pheochromocytoma and Paraganglioma (PCPG); Prostate adenocarcinoma (PRAD); Rectum adenocarcinoma (READ); Sarcoma (SARC); Skin Cutaneous Melanoma (SKCM); Stomach adenocarcinoma (STAD); Testicular Germ Cell Tumors (TGCT); Thyroid carcinoma (THCA); Thymoma (THYM); Uterine Corpus Endometrial Carcinoma (UCEC); Uterine Carcinosarcoma (UCS); Uveal Melanoma (UVM). TPM: transcript per million. RPPA: reverse-phase protein array. **Figure S4.** EGFR expression in head and neck squamous cell carcinoma (HNSC) tumors of the TCGA cohort compared to normal (non-tumor) adjacent tissue, based on sample types (A), tumor grade (B), or individual cancer stage (C). Gene expression data were downloaded from UALCAN (<http://ualcan.path.uab.edu/analysis.html>). pVal versus Normal: * < 0.05; ** < 0.001; *** < 0.0001. Tumor grades are according to the NIH National Cancer Institute (<https://www.cancer.gov/about-cancer/diagnosis-staging/diagnosis/tumor-grade>). Tumor stages are based on Neoplasm Disease Stage American Joint Committee on Cancer Codes (<https://www.facs.org/quality-programs/cancer-programs/american-joint-committee-on-cancer/cancer-staging-systems/>). **Figure S5.** Cell viability (XTT assay) of Cal33, Cal27 or FaDu cells treated with increasing concentrations of non-loaded NP (A), ACNP (B) or Cetuximab alone (C) for 72 hours. Mean \pm SEM. A-B) The gray-shaded area denotes the range of the IC50 concentrations of Alpelisib loaded in the nanoparticles: 0.02-0.6 μM Alpelisib \cong 4.8-144 $\mu\text{g}/\text{mL}$ NP or ACNP. **Figure S6.** A) Cell viability (XTT assay) curve of Cal33 cells treated with increasing concentrations of free Alpelisib for 24 hours as shown in Fig. 6B. Mean \pm SEM. The red dots indicate the concentrations used for experiments in (B) and (C), which followed a similar scheme to that of Fig. 6A. B) Cell viability analysis of Cal33 cells treated with the indicated concentrations of free Alpelisib or NP-Alpelisib for 6 hours (followed by 18 h incubation with drug-free media) or 24 hours. The dotted line indicates 100% cell survival of untreated cells. Cells "0 μM " were treated with the vehicle of Alpelisib (DMSO) or with empty nanoparticles at equivalent concentrations to those used in the experiments. Mean \pm SEM. Ordinary

one-way ANOVA multiple comparisons: * pVal < 0.5, *** pVal < 0.0001 versus untreated cells. C) Western blot (WB) analysis for the indicated proteins/phosphoproteins of Cal33 cells treated with 1.5 μ M Alpelisib. **Figure S7**. WB analysis for EGFR and phosphoEGFR of Cal33 cells treated with 0.5 μ M Alpelisib for 24 hours. **Figure S8**. 1H spectrum of PLA in CDC13 at room temperature obtained by Ring-Opening Polymerization and used as raw material for the generation of polymeric nanoparticles. **Figure S9**. Blots 1-3. Complete blots from Figure 6D and Supplementary Figure S7. **Figure S10**. Blots 4-6. Complete blots from Supplementary Figure S6C.

Acknowledgements

The authors thank Montse Grau (supervisor of the animal facilities in Hospital 12 de Octubre) for assistance with in vivo imaging. We thank Norman Feltz for proofreading the article.

Author contributions

All authors have made substantial contributions to the work discussed in this publication. CA-M and CL designed the study and wrote the manuscript. CA-M, CL and IB supervised the study. CA-M, CL and AO provided the funding. AJ, CS, AdC, IS, JP, PC-C. performed the experiments and analyzed the data. All authors contributed to the preparation of the manuscript. All authors read and approved the final manuscript.

Funding

This work was supported by Instituto de Salud Carlos III (ISCIII) and co-funded by the European Union [Grant Numbers PI18/00263, PI19/00808, PI21/00208 and CB16/12/00228]. J.P. was supported by a FEDER co-funded grant from the Ministerio de Ciencia, Innovación y Universidades [Grant Number PEJ2018-002040-A]. We also gratefully acknowledge the financial support; grant PID2020-117788RB-I00 and PID2019-106068 GB-I00 funded by MCIN/AEI/10.13039/501100011033 and SBPLY/21/180501/000050 and SBPLY/21/180501/000076 funded by JCCM and by EU through Fondo Europeo de Desarrollo Regional. A.dC-B. acknowledges the Universidad de Castilla-La Mancha (UCLM) for the PhD Fellowship. The CRIS Cancer Foundation and ACEPAIN.

Availability of data and materials

All data generated or analyzed during this study are included in this published article [and its supplementary information files]. Additionally, the datasets analyzed in Additional file 1: Figs. S3 and S4 are available in the TCGA Research Network, <https://www.cancer.gov/tcga>.

Declarations

Ethics approval and consent to participate

This study was conducted in accordance with the Declaration of Helsinki. All animal experiments were conducted in compliance with CIEMAT Institutional Animal Care and Use Committee guidelines and approved by the Animal Welfare Department (protocol: PROEX 045.8/21, date of approval: 12/02/2021).

Consent for publication

Not applicable.

Competing interests

The authors declare that they have no competing interests.

Author details

¹Unidad NanoDrug, Centro Regional de Investigaciones Biomédicas, Universidad de Castilla-La Mancha, 02008 Albacete, Spain. ²Unidad de Innovación Biomédica, CIEMAT (ed 70A), Ave Complutense 40, 28040 Madrid, Spain. ³Instituto de Investigación Sanitaria Hospital 12 de Octubre (imas12), Ave Córdoba s/n, 28041 Madrid, Spain. ⁴Centro de Investigación Biomédica en Red de Cáncer (CIBERONC), Ave Monforte de Lemos 3-5, 28029 Madrid, Spain. ⁵Departamento Química Inorgánica, Orgánica y Bioquímica, Facultad de Farmacia de Albacete-Centro de Innovación en Química Avanzada (ORFEO-CINQA), Universidad de Castilla-La Mancha, 02008 Albacete, Spain. ⁶Departamento Química-Física. Facultad de Farmacia de Albacete, Universidad de Castilla-La Mancha, 02008 Albacete, Spain. ⁷Experimental Therapeutics Unit, Hospital Clínico San Carlos, IdISSC, Fundación Jiménez Díaz, START, 28040 Madrid, Spain. ⁸Laboratorio de Virología Molecular, Centro Regional de Investigaciones Biomédicas, Universidad de Castilla-La Mancha, 02008, Albacete, Spain. ⁹Facultad de Farmacia de Albacete, Universidad de Castilla-La Mancha, 02008 Albacete, Spain.

Received: 26 January 2023 Accepted: 18 March 2023

Published online: 29 March 2023

References

- Broadbridge VT, Karapetis CS, Price TJ (2012) Cetuximab in metastatic colorectal cancer. *Expert Rev Anticancer Ther* 12:555–565. <https://doi.org/10.1586/era.12.25>
- Cancer Genome Atlas Network (2015) Comprehensive genomic characterization of head and neck squamous cell carcinomas. *Nature* 517:576–582. <https://doi.org/10.1038/nature14129>
- Cancer Genome Atlas Research Network (2012) Comprehensive genomic characterization of squamous cell lung cancers. *Nature* 489:519–525. <https://doi.org/10.1038/nature11404>

- Chandrashekar DS, Basha B, Balasubramanya SAH, Creighton CJ, Ponce-Rodriguez I, Chakravarthi B, Varambally S (2017) UALCAN: a portal for facilitating tumor subgroup gene expression and survival analyses. *Neoplasia* 19:649–658. <https://doi.org/10.1016/j.neo.2017.05.002>
- Chandrashekar DS et al (2022) UALCAN: an update to the integrated cancer data analysis platform. *Neoplasia* 25:18–27. <https://doi.org/10.1016/j.neo.2022.01.001>
- Cimas FJ et al (2020) Controlled delivery of BET-PROTACs in vitro evaluation of MZ1-loaded polymeric antibody conjugated nanoparticles in breast cancer. *Pharmaceutics* 12:986. <https://doi.org/10.3390/pharmaceutics12100986>
- Day D et al (2020) Phase I trial of alpelisib in combination with concurrent cisplatin-based chemoradiotherapy in patients with locoregionally advanced squamous cell carcinoma of the head and neck. *Oral Oncol* 108:104753. <https://doi.org/10.1016/j.oraloncology.2020.104753>
- De Buck SS, Jakab A, Boehm M, Bootle D, Juric D, Quadt C, Goggin TK (2014) Population pharmacokinetics and pharmacodynamics of BYL719, a phosphoinositide 3-kinase antagonist, in adult patients with advanced solid malignancies. *Br J Clin Pharmacol* 78:543–555. <https://doi.org/10.1111/bcp.12378>
- Dunn LA et al (2020) A phase 1b study of Cetuximab and BYL719 (Alpelisib) concurrent with intensity modulated radiation therapy in stage III-IVB head and neck squamous cell carcinoma. *Int J Radiat Oncol Biol Phys* 106:564–570. <https://doi.org/10.1016/j.ijrobp.2019.09.050>
- Elkabetz M et al (2015) AXL mediates resistance to PI3K α inhibition by activating the EGFR/PKC/mTOR axis in head and neck and esophageal squamous cell carcinomas. *Cancer Cell* 27:533–546. <https://doi.org/10.1016/j.ccell.2015.03.010>
- Ferlay J et al (2015) Cancer incidence and mortality worldwide: sources, methods and major patterns in GLOBOCAN 2012. *Int J Cancer* 136:E359–386. <https://doi.org/10.1002/ijc.29210>
- Fritsch C et al (2014) Characterization of the novel and specific PI3K α inhibitor NVP-BYL719 and development of the patient stratification strategy for clinical trials. *Mol Cancer Ther* 13:1117–1129. <https://doi.org/10.1158/1535-7163.MCT-13-0865>
- Garcia-Escudero R et al (2018) Overexpression of PIK3CA in head and neck squamous cell carcinoma is associated with poor outcome and activation of the YAP pathway. *Oral Oncol* 79:55–63. <https://doi.org/10.1016/j.oraloncology.2018.02.014>
- Ionna F et al (2021) Recurrent/metastatic squamous cell carcinoma of the head and neck: a big and intriguing challenge which may be resolved by integrated treatments combining locoregional and systemic therapies. *Cancers* 13:2371. <https://doi.org/10.3390/cancers13102371>
- Johnson DE, Burtneis B, Leemans CR, Lui VWY, Bauman JE, Grandis JR (2020) Head and neck squamous cell carcinoma. *Nat Rev Dis Primers* 6:92. <https://doi.org/10.1038/s41572-020-00224-3>
- Juan A, Cimas FJ, Bravo I, Pandiella A, Ocana A, Alonso-Moreno C (2020) Antibody conjugation of nanoparticles as therapeutics for breast cancer treatment. *Int J Mol Sci* 21:6018. <https://doi.org/10.3390/ijms21176018>
- Juan A et al (2022) Enhanced antitumoral activity of encapsulated BET inhibitors when combined with PARP inhibitors for the treatment of triple-negative breast and ovarian cancers. *Cancers* 14:4474. <https://doi.org/10.3390/cancers14184474>
- Juric D et al (2018) Phosphatidylinositol 3-kinase α -selective inhibition with alpelisib (BYL719) in PIK3CA-altered solid tumors: results from the first-in-human study. *J Clin Oncol* 36:1291–1299. <https://doi.org/10.1200/JCO.2017.72.7107>
- Markham A (2019) Alpelisib: first global approval. *Drugs* 79:1249–1253. <https://doi.org/10.1007/s40265-019-01161-6>
- Martin D et al (2014) The head and neck cancer cell oncogene: a platform for the development of precision molecular therapies. *Oncotarget* 5:8906–8923. <https://doi.org/10.18632/oncotarget.2417>
- Massacesi C et al (2016) PI3K inhibitors as new cancer therapeutics: implications for clinical trial design. *Onco Targets Ther* 9:203–210. <https://doi.org/10.2147/OTT.S89967>
- Mazumdar S, Chitkara D, Mittal A (2021) Exploration and insights into the cellular internalization and intracellular fate of amphiphilic polymeric nanocarriers. *Acta Pharmaceutica Sinica B* 11:903–924. <https://doi.org/10.1016/j.apsb.2021.02.019>
- Miyamoto Y et al (2019) Epidermal growth factor receptor-targeted molecular imaging of colorectal tumors: detection and treatment evaluation of tumors in animal models. *Cancer Sci* 110:1921–1930. <https://doi.org/10.1111/cas.14020>
- Mizrachi A et al (2017) Tumour-specific PI3K inhibition via nanoparticle-targeted delivery in head and neck squamous cell carcinoma. *Nat Commun* 8:14292. <https://doi.org/10.1038/ncomms14292>
- Niza E, Ocana A, Castro-Osma JA, Bravo I, Alonso-Moreno C (2021) Polyester polymeric nanoparticles as platforms in the development of novel nanomedicines for cancer treatment. *Cancers*. <https://doi.org/10.3390/cancers13143387>
- Price KA, Cohen EE (2012) Current treatment options for metastatic head and neck cancer. *Curr Treat Options Oncol* 13:35–46. <https://doi.org/10.1007/s11864-011-0176-y>
- Rabinowitz G, Haddad RI (2012) Overcoming resistance to EGFR inhibitor in head and neck cancer: a review of the literature. *Oral Oncol* 48:1085–1089. <https://doi.org/10.1016/j.oraloncology.2012.06.016>
- Rabney A, Baum K, Pitts D (2006) Cetuximab approved by FDA for treatment of head and neck squamous cell cancer. *Cancer Biol Ther* 5:340–342
- Ren J, Han KY (2021) 2.5D microscopy: fast, high-throughput imaging via volumetric projection for quantitative subcellular analysis. *ACS Photonics* 8:933–942. <https://doi.org/10.1021/acsp Photonics.1c00012>
- Roncato F et al (2018) Improvement and extension of anti-EGFR targeting in breast cancer therapy by integration with the Avidin-nucleic-acid-nano-assemblies. *Nat Commun* 9:4070. <https://doi.org/10.1038/s41467-018-06602-6>
- Sánchez-Barba LF et al (2007) Well-defined alkyl heteroscorpionate magnesium complexes as excellent initiators for the ROP of cyclic esters. *Organometallics* 26:6403–6411
- Sánchez-Barba LF et al (2009) Synthesis, structures and ring-opening polymerization studies of new zinc chloride and amide complexes supported by amidinate heteroscorpionate ligands. *Dalton Trans.* <https://doi.org/10.1039/b910048b>
- Sanchez-Vega F et al (2018) Oncogenic signaling pathways in the cancer genome atlas. *Cell* 173:321–337 e310. <https://doi.org/10.1016/j.cell.2018.03.035>
- Segrelles C, Contreras D, Navarro EM, Gutierrez-Munoz C, Garcia-Escudero R, Paramio JM, Lorz C (2018) Bosutinib inhibits EGFR activation in head and neck cancer. *Int J Mol Sci* 19:1824. <https://doi.org/10.3390/ijms19071824>

- Velazquez-Lam E et al (2022) Antitumor applications of polyphenol-conjugated turnip mosaic virus-derived nanoparticles. *Nanomedicine (lond)* 17:999–1012. <https://doi.org/10.2217/nnm-2022-0067>
- Vivanco I, Sawyers CL (2002) The phosphatidylinositol 3-kinase AKT pathway in human cancer. *Nat Rev Cancer* 2:489–501. <https://doi.org/10.1038/nrc839>
- Wang XB, Zhou HY (2015) Molecularly targeted gemcitabine-loaded nanoparticulate system towards the treatment of EGFR overexpressing lung cancer. *Biomed Pharmacother* 70:123–128. <https://doi.org/10.1016/j.biopha.2015.01.008>
- Wang Z, Valera JC, Zhao X, Chen Q, Gutkind JS (2017) mTOR co-targeting strategies for head and neck cancer therapy. *Cancer Metastasis Rev* 36:491–502. <https://doi.org/10.1007/s10555-017-9688-7>

Publisher's Note

Springer Nature remains neutral with regard to jurisdictional claims in published maps and institutional affiliations.

Ready to submit your research? Choose BMC and benefit from:

- fast, convenient online submission
- thorough peer review by experienced researchers in your field
- rapid publication on acceptance
- support for research data, including large and complex data types
- gold Open Access which fosters wider collaboration and increased citations
- maximum visibility for your research: over 100M website views per year

At BMC, research is always in progress.

Learn more biomedcentral.com/submissions

